

Understanding Intramolecular Electron Transfer in Ferredoxin: A Molecular Dynamics Study

Ming-Liang Tan,[†] Elizabeth A. Dolan,[‡] and Toshiko Ichiye^{*,†}

Department of Chemistry, Georgetown University, Washington, D.C. 20057-1227, and School of Molecular Biosciences, Washington State University, Pullman, Washington 99164-4660

Received: August 11, 2004; In Final Form: September 27, 2004

An important question about electron-transfer proteins is how the environment of the redox site created by the protein's matrix affects their electron-transfer properties. Here, we investigate intramolecular electron transfer in the [4Fe–4S] ferredoxins, which are a class of iron–sulfur electron-transfer proteins found in numerous electron transport chains, including the photosynthetic pathway. These proteins are characterized by having two [4Fe–4S] clusters, often but not always with the same reduction potential, and by the pseudo-2-fold symmetry of the protein backbone. The nuclear polarization is calculated from molecular dynamics simulations of *Clostridium acidiurici* ferredoxin, with a total of 6 ns of simulation, and is then used to calculate free energy reaction curves. In addition, we present here a new method, referred to as the Gaussian parabola method, for obtaining the reaction energy ΔG° and the reorganization energy λ from the mean and fluctuations of the polarization, which is based on the linear response of a system with Gaussian fluctuations. For ferredoxin, the calculated outer sphere λ is small (<200 meV) and is consistent with the lack of temperature dependence in experimental measurements of rates for this protein; however, the rate calculated from the calculated λ is consistent with experimental values if the inner sphere λ is large. The calculations also indicate that the contribution of the protein to λ is smaller than that of the solvent, which implies that the protein enhances the rate of electron transfer by providing an environment that has a low reorganization energy.

Introduction

Electron-transfer proteins serve a vital role in the transport and utilization of cellular energy. They are ubiquitous to all life and are found in the pathways of cellular respiration, photosynthesis, and nitrogen fixation. These proteins use oxidation–reduction chemistry to transfer an electron from a donor site to an acceptor site and thus can be described by theories for electron transfer,^{1,2} in which the environment is assumed to affect the rate of an electron-transfer reaction. Specifically, in Marcus theory, the polarization of the environment is assumed to respond linearly to changes in charge, which means that the environmental free energy functions are quadratic or parabolic, with the same curvature.

Free energy curves for electron-transfer reactions have been studied from computer simulations with methods pioneered by Warshel and co-workers.^{3–6} For example, the exchange between two benzene-like solutes,⁵ ferric–ferrous self-exchange,^{7–9} rubredoxin self-exchange,¹⁰ and the photosynthetic reaction center^{11–13} have all been studied by using these methods. In these studies, the assumption of a quadratic free energy curve was reasonable, although a nonlinear response leading to nonparabolic free energy curves becomes apparent under certain conditions, such as the self-exchange of electrons for small ions.⁹

Electron-transfer reactions are highly efficient in biological systems, transferring electrons over relatively large distances and with very fast rates.¹⁴ For example, electrons can be

transferred between reduced hemes over distances of 10 to 20 Å at physiologically significant rates.¹⁴ The means by which electron-transfer proteins control these reactions is of great interest, both for basic understanding of these systems and also for bioengineering applications. Specifically, an important question is how the protein is able to provide an environment that gives rise to small activation energies. While mutations along the entire pathway between the two sites may affect the electronic coupling, mutations close to the redox sites also have been shown to affect the thermodynamic properties of electron transfer¹⁵ and thus are more likely to affect ΔG^\ddagger due to the contributions of the reorganization energy. Although a significant amount of work has been performed on electron transfer between ruthenium-modified histidines and natural redox centers in proteins,^{16,17} the focus here is on electron transfer between natural sites in proteins, namely, the ferredoxins.

Ferredoxins (Fd) are a group of small (6 to 12 kDa, 55 to 100 aa) iron–sulfur electron-transfer proteins that are found in a wide range of biological functions, including nitrogen fixation,¹⁸ proton transfer,¹⁹ and reduction–oxidation reactions in the cytoplasm.^{20,21} [4Fe–4S]-type ferredoxins consist of a $\beta\alpha\beta-\beta\alpha\beta$ fold motif containing either one or two cubane-like [4Fe–4S] clusters, where the basic structure consists of two iron sulfur clusters and a quasi-2-fold symmetry of the backbone (Figure 1).²² The iron atoms in the redox cluster of ferredoxin are ligated to the rest of the protein by cysteinyl residues with a ligation pattern Cys¹-X₂-Cys²-X₂-Cys³-X_n-Cys⁴, where superscripts indicate the four ligands of one cluster, X is any residue, and n indicates that the fourth redox site ligand is far removed (either upstream or downstream) in sequence from the first three

* Address correspondence to this author. E-mail: ti9@georgetown.edu. Phone: (202) 687-3724. Fax: (202) 687-6209.

[†] Georgetown University.

[‡] Washington State University.

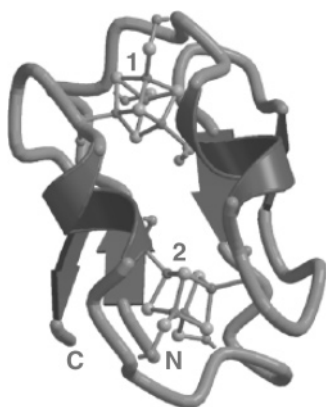


Figure 1. Ribbon diagram of *Clostridium acidurici* ferredoxin (2FDN) containing an $\alpha\beta\beta-\alpha\beta\beta$ pseudosymmetric backbone fold. The two $[4\text{Fe}-4\text{S}]$ clusters are shown in a ball-and-stick model and are labeled as clusters 1 and 2.

ligands.²³ The two-cluster ferredoxins have two of these ligation patterns, which can alternatively be described by the sequence motif $\text{Cys}^1\text{-X}_2\text{-Cys}^2\text{-X}_2\text{-Cys}^3\text{-X-Cys}^4$, where the superscript 4' indicates a ligand of a different cluster than the unprimed superscripts. Ferredoxins with two $[4\text{Fe}-4\text{S}]$ redox sites are known to transfer electrons between the sites²⁴ and the transfer is fast on the NMR time scale ($k > 10^4 \text{ s}^{-1}$).²⁵ The relevant redox couple for the $[4\text{Fe}-4\text{S}]$ ferredoxins is $[\text{Fe}_4\text{S}_4(\text{SR})_4]^{2-/\beta-}$, which has characteristic potentials from -645 to 0 mV .²⁶ The reduction potentials may be the same for both sites or different by as much as 192 mV .²⁷ High-resolution ($<2.3 \text{ \AA}$) X-ray crystal or NMR solution structures of four one-cluster and seven two-cluster ferredoxins, plus a number of mutant ferredoxins, have been solved and are available in the Brookhaven Protein Data Bank (PDB).²⁸ Additionally, the sequences of approximately 120 species are available.

Here, the intramolecular electron-transfer reaction of ferredoxin is studied, specifically, the transfer of an extra electron between the two oxidized $[4\text{Fe}-4\text{S}]$ clusters (or $[\text{Fe}_4\text{S}_4(\text{SR})_4]^{2-}$), which is advantageous for several reasons. First, the donor and the acceptor are bound and therefore no orientation effects need to be considered.^{29,30} Second, the distance between the donor and acceptor can be calculated from the crystal structures in the PDB.³¹ Third, ferredoxins are well characterized, with intramolecular transfer rates on the order of 10^6 s^{-1} .¹⁵ Finally, computational studies have identified sequence determinants of the reduction potential.³² Specifically, *Clostridium acidurici* ferredoxin (Ca Fd) is studied in this work. Ca Fd is an example of the simplest form of ferredoxin (Fajardo and Ichiye, to be published), and a high-resolution crystal structure (0.98 \AA)³¹ is available in the PDB. The protein is very symmetric and thus the redox sites are in relatively similar environments with similar reduction potentials of approximately -420 mV .³³ The similar reduction potentials indicate that the driving force should be relatively small; however, transfer has been shown to be fast on the NMR time scale and theoretical electron-transfer pathways have been calculated.^{15,29-31}

In this work, molecular dynamics simulations of Ca ferredoxin are performed with different oxidation states of the redox sites. The nuclear polarization of the protein around the redox site is calculated from the trajectories and is then used to estimate the free energy curve, driving force, activation energy, reorganization energy, and electron transfer rate for the electron-transfer reaction in Ca Fd. These parameters are calculated from the simulation both via the standard method and a new method. The standard method involves a least-squares fit of a parabola

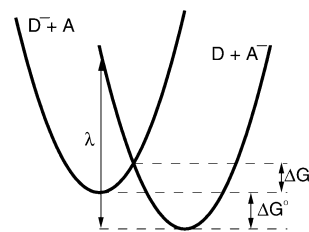


Figure 2. A schematic representation of potential energy curves for the electron-transfer reaction $D^- + A \rightarrow D + A^-$, where D indicates the donor and A indicates the acceptor, ΔG° is the driving force, ΔG^\ddagger is the activation barrier, and λ is the reorganization energy.

to a free energy curve for the reaction calculated from a histogram of the polarization energies. The new method presented here relates the parameters directly to the mean and fluctuation of the polarization energies by making the assumption that the polarization energies follow a Gaussian distribution. Both methods are outlined fully in the Methods section.

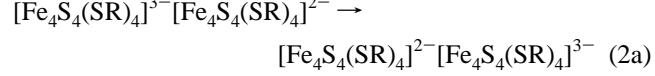
Methods

Theory.

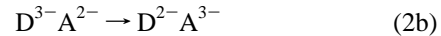
Consider the following electron-transfer reaction,



where a donor (D) transfers an electron to an acceptor (A). In ferredoxin, the donor and the acceptor are the two respective iron-sulfur clusters, such that



or



The letters R and P will be used to refer to the reactants ($\text{D}^{3-}\text{A}^{2-}$) and products ($\text{D}^{2-}\text{A}^{3-}$) of eq 2, respectively, and $\Delta G_a(X)$ will refer to the value of the free energy as a function of the reaction coordinate X with the donor and acceptor in state a; i.e., a = R, P. Marcus theory assumes that the reaction coordinate is the polarization of the environment and that the free energy for a given state as a function of the polarization coordinate is parabolic, as shown in Figure 2, where $\Delta G_R(X)$ is the free energy curve of the reactants, $\Delta G_P(X)$ is the free energy curve of the products, ΔG^\ddagger is the activation barrier, ΔG° is the driving force, and λ is the reorganization energy.¹ This leads to the well-known Marcus relation

$$\Delta G^\ddagger = \frac{(\lambda + \Delta G^\circ)^2}{4\lambda} \quad (3)$$

where the activation barrier is shown to be a function of the driving force and the reorganization energy.

The free energy curves are constructed by using the molecular version of Marcus theory, as developed by Warshel and co-workers.³⁻⁶ This method calculates the free energy curves $\Delta G_R(X)$ and $\Delta G_P(X)$ from the ratio of the probability of being at X on the reaction coordinate versus the probability of being at the minimum,

$$\Delta G_R(X) = -k_B T \ln[P_R(X)] \quad (4a)$$

$$\Delta G_P(X) = -k_B T \ln[P_P(X)] + \Delta G^\circ \quad (4b)$$

where $P(X)$ is the probability of X , k_B is Boltzmann's constant,

and T is the temperature. The functions $P(X)$ can be obtained from simulations by histograms of reaction coordinate X . However, X must be defined explicitly.

For the reaction coordinate X , a global reaction coordinate for the many-dimensional coordinate space of this system is defined rather than the conventional local reaction coordinate.³⁴ Here, the reaction coordinate is the polarization coordinate, defined as the difference in the electrostatic potential energy (or electrostatic energy gap) between reactant charge state, D^3-A^{2-} , and product charge state, D^2-A^{3-} , for a given nuclear configuration \mathbf{r} , following the method by Warshel and co-workers,¹³ such that

$$\Delta V(\mathbf{r}) = V_p(\mathbf{r}) - V_r(\mathbf{r}) \quad (5a)$$

and

$$V_a = \sum_{\gamma=D,A} \sum_i \sum_j (q_{\gamma i} q_j) / r_{ij} \quad (5b)$$

where $a = R, P$. V_a is the electrostatic energy, $q_{\gamma i}$ is the partial charge at the center of the atom i in the respective redox site γ , q_j is the partial charge at the center of the atom j in the environment, and r_{ij} is the distance between atoms i and j . The atoms of the redox site here are chosen as all atoms of the cluster including the cysteinyl S and C. The free energy G of the entire system of reacting species and solvent can be defined along the global reaction coordinate. Combining eqs 4a and 4b with eq 5a, the relationship between the free energy surfaces and the global reaction coordinate, defined as the electrostatic energy gap between two charge states, is

$$\Delta G_R(\Delta V) = -k_B T \ln\{P_R[\Delta V(\mathbf{r}_R)]\} \quad (6a)$$

$$\Delta G_P(\Delta V) = -k_B T \ln\{P_P[\Delta V(\mathbf{r}_P)]\} + \Delta G^\circ \quad (6b)$$

where \mathbf{r}_R are the nuclear configurations from the molecular dynamics trajectories of the reactant state, and \mathbf{r}_P are the nuclear configurations from the molecular dynamics trajectories of the product state.

Molecular Dynamics Simulations. Molecular dynamics simulations were carried out with use of the molecular mechanics package CHARMM29b2.³⁵ The simulations were carried out in the microcanonical ensemble with a target temperature of 300 K, using the particle mesh Ewald (PME) summation algorithm.³⁶ The time step was 1 fs. Cubic boundary conditions of $45 \times 45 \times 45 \text{ \AA}^3$ were utilized, with a grid spacing of 0.9375 Å, a β -spline coefficient equal to 6, and a κ value of 0.34. The force field parameters consisted of the CHARMM19 parameters³⁵ plus additional parameters for the iron–sulfur redox site as described elsewhere.³² All nonpolar hydrogens were treated via the extended atom model as part of the heavy atom to which they are attached, and all bonds containing hydrogen were held at their equilibrium bond lengths by using the SHAKE algorithm.³⁷ No atomic polarizability was included and a dielectric constant of 1 was used throughout the simulations. Our experience with different parameters indicates that a different force field would not result in qualitative differences.³⁸

The high-resolution crystal structure (0.94 Å) of the fully oxidized structure for Ca Fd was obtained from the Brookhaven Protein Data Bank²⁸ (2FDN).³¹ In what follows, the donor (D) refers to the site ligated by residues 8, 11, 14, and 47 (cluster 1) and the acceptor (A) refers to the site ligated by residues 37, 40, 43, and 18 (cluster 2). Two forms of the protein were simulated, D^3-A^{2-} and D^2-A^{3-} , which utilized the fully oxidized structure as starting structures but with the appropriate

oxidized and reduced potential energy parameters for each site. The protein was completely solvated in a $45 \times 45 \times 45 \text{ \AA}^3$ box of preequilibrated TIP3P³⁹ water as implemented in CHARMM. All solvent waters within 2.6 Å of any nonhydrogen protein atom or crystal water oxygen were then deleted, resulting in 2782 total waters. Next, the solvent was relaxed slightly by 50 steps of steepest descent energy minimization followed by 2.0 ps of molecular dynamics with Gaussian assignment of velocities every 0.2 ps in which only the solvent was allowed to move and the protein remained fixed. Next, counterions^{40–42} were added by replacing a water molecule with an ion near each charged group (a sodium ion for the negatively charged side chains, the C-terminus, and the redox clusters, and a chlorine ion for the positively charged side chains and the N-terminus) of the protein to make the system net neutral. Thus, the final system consisted of 2765 TIP3P waters, 15 Na⁺ ions, 2 Cl⁻ ions, and the protein. The solvent environment was equilibrated by fixing the protein while the counterion and solvent velocities were propagated for 60 ps, during which time the velocities were scaled every 0.2 ps to a target temperature of 300 ± 5 K. Finally, the entire system was equilibrated, where velocities were assigned to the entire system according to a Gaussian distribution every 200 fs. Following this assignment, the velocities were allowed to scale every 200 fs if the temperature exceeded 300 ± 5 K until there was no scaling for at least 20 ps. The amount of scaling was approximately 180 ps for both systems. The system was then allowed to run unrestrained for 3.3 ns and the last 3 ns of data were analyzed for each system.

Free Energy Curves. The electrostatic potential energy V at each time step in the trajectory data was calculated by using Coulomb's law. The differences in the electrostatic potential energy ΔV between two donor and acceptor charge states, i.e., D^3-A^{2-} and D^2-A^{3-} , were then calculated for each of the reactant and product nuclear configurations. The free energy curves were then constructed by two methods outlined below.

The first method involves fitting histograms of the data and will be referred to as “fit” parabolas. First, histograms of the energy gap ΔV were constructed by using 20 equally spaced energetic values. Next, the free energy curves for the reactant and product systems were calculated via eqs 6a and 6b. Finally, the free energy curves from the histograms were fit by least squares to parabolic functions. The driving force, ΔG° , was calculated simply by setting the reactant $\Delta G_R(\Delta V)$ equal to the product $\Delta G_P(\Delta V)$ at $\Delta V = 0$, using the method of Warshel and co-workers.¹³ Then, the activation energy, ΔG^\ddagger , was calculated from the fitted curves by finding the height of the reactant parabolic curve at the point where the reactant and product surfaces intersect. Next, the reorganization energy, λ , was calculated from the activation energy and the driving force by using the Marcus relation (eq 3). In addition, the reorganization energy of reactants, λ_R , was calculated as the difference in the free energy of the reactants (i.e. the reactant curve) at the reactant minimum versus the product minimum, and the reorganization energy of the products, λ_P , was calculated as the difference in the free energy of the products (i.e. the product curve) at the product minimum versus the reactant minimum. To estimate the relative error in calculating these parameters, each of the 3-ns simulation data was equally divided into three segments of 1 ns data. Each segment was then used to construct individual free energy curves separately and the standard relative errors were estimated for the quantities calculated.

The free energy curves can also be constructed by using a few parameters from the MD simulation. On the basis of

previous work,⁴³ the parabolas of the reactant and product were constructed from the mean values and the dynamic fluctuations of the reaction coordinate $\mu_a = \langle X \rangle_a$ and $\sigma_a^2 = \langle (X - \langle X_a \rangle)^2 \rangle_a$, respectively, for state $a = R, P$, and will be referred to as the “Gaussian” parabolas. The previous work was based on the linear response of a system with Gaussian fluctuations, which leads to further relationships for parameters describing the parabolic free energy curves, namely λ , ΔG° , and ΔG^\ddagger . The minima of the parabolas are at $X_a = \mu_a$ and the corresponding force constants of the parabolas are given by $k_a = k_B T / \sigma_a^2$, where k_B is the Boltzmann constant and T is the temperature so that the free energy is given by

$$\Delta G_R(X) = \frac{1}{2} k_R (X - X_R)^2 \quad (7a)$$

$$\Delta G_P(X) = \frac{1}{2} k_P (X - X_P)^2 + \Delta G^\circ \quad (7b)$$

If $k_P = k_R = k$, the relationship is simplified greatly. The reorganization energy is thus

$$\lambda_P = \lambda_R = \lambda = \frac{1}{2} k (X_P - X_R)^2 \quad (8)$$

The transition state at $X = X^\ddagger$ is defined by

$$X^\ddagger = \frac{k(X_P^2 - X_R^2)/2 + \Delta G^\circ}{k(X_P - X_R)} \quad (9)$$

and the activation energy is given by

$$\Delta G_{R \rightarrow P}^\ddagger = \Delta G_R(X^\ddagger) = \frac{(\lambda + \Delta G^\circ)^2}{4\lambda} \quad (10)$$

i.e., the Marcus relation. Furthermore, if $X^\ddagger = 0$, then from eq 9

$$\Delta G^\circ = \frac{1}{2} k (X_R^2 - X_P^2) \quad (11)$$

However, if $k_P \neq k_R$, the reorganization energies are different for the products and reactants

$$\lambda_a = \frac{1}{2} k_a (X_P - X_R)^2 \quad (12)$$

where λ_P is the reorganization energy of state from $X = X_R$ to $X = X_P$ and λ_R is defined analogously. The transition state is now

$$X^\ddagger = \frac{(k_P X_P - k_R X_R) \pm [k_P k_R (X_P - X_R)^2 - 2(k_P - k_R) \Delta G^\circ]^{1/2}}{k_P - k_R} \quad (13)$$

Although a closed form expression for $\Delta G_{R \rightarrow P}^\ddagger$ may be obtained from substituting eq 13 into $\Delta G_R(X^\ddagger)$, an equation related to eq 9 is obtained by substituting

$$X^\ddagger = \frac{(k_P X_P^2 - k_R X_R^2)/2 + \Delta G^\circ + (k_P - k_R) X^\ddagger / 2}{k_P X_P - k_R X_R} \quad (14)$$

to obtain

$$\Delta G^\ddagger = \frac{(\lambda_{(1)} + \Delta G^\circ + (k_P - k_R) X^\ddagger / 2)^2}{4\lambda_{(2)}} \quad (15)$$

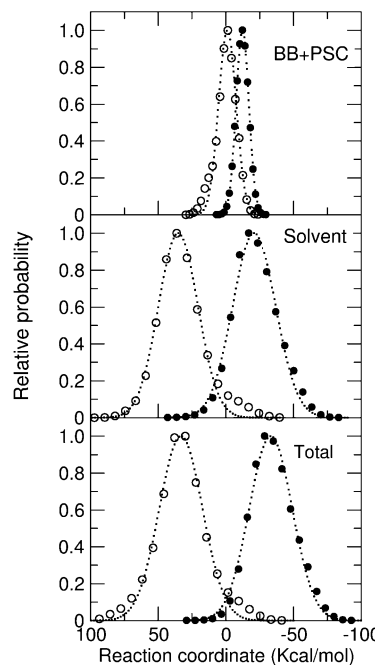


Figure 3. Distribution of electrostatic energy difference between $D^{3-}A^{2-}$ and $D^{2-}A^{3-}$ charge states for reactant (\circ) and product (\bullet) systems. The dotted curves are corresponding Gaussian fits. The top panel is for the protein backbone and polar side chains (BB+PSC); the middle panel is for the solvent plus counterions and charged side chains (Solvent); and the bottom panel is for the total system (Total).

where $\lambda_{(1)} = (k_P X_P^2 - 2k_P X_P X_R + k_R X_R^2)/2$ and $\lambda_{(2)} = (k_P X_P - k_R X_R)^2/2k_R$, which easily reduces to eq 10 if $k_P = k_R$. This also means that a value of λ calculated by substituting ΔG° and ΔG^\ddagger into eq 10 will give a λ that is related to the average of λ_P and λ_R . Furthermore, if $X^\ddagger = 0$, then from eq 14

$$\Delta G^\circ = \frac{1}{2} (k_R X_R^2 - k_P X_P^2) \quad (16)$$

In this work, ΔG° is calculated by using eq 16, λ_P and λ_R by using eq 12, λ by using eq 8, and ΔG^\ddagger by using eq 15.

Results

Fit Parabolas The distributions of the reaction coordinate for both the reactants ($D^{3-}A^{2-}$) and products ($D^{2-}A^{3-}$) (Figure 3) were obtained by constructing the corresponding histograms of the electrostatic energy gap ΔV (see Methods). The results are analyzed for the total system, the backbone plus polar side chains, and the solvent plus counterions and charged side chains. Although there is obviously coupling between various components, this separation gives an indication of the contribution of protein versus solvent, which will be addressed in the Discussion. Previous work⁴⁴ has indicated the contribution of the charged side chains is highly correlated with the counterions so that they are included with the solvent rather than the proteins, and the counterions cannot be considered independent of the solvent because they are highly coupled as well. All the distributions are fit well by the Gaussian distribution. The backbone and polar side chains (Figure 3, top panel) have a narrow probability distribution when compared to both solvent plus counterions and charged side chains (Figure 3, middle panel) and the total system (Figure 3, bottom panel), since the protein is more constrained than the solvent environment. This indicates that the wide distribution of the electrostatic energy of the total system is mainly due to the flexible solvent environment.

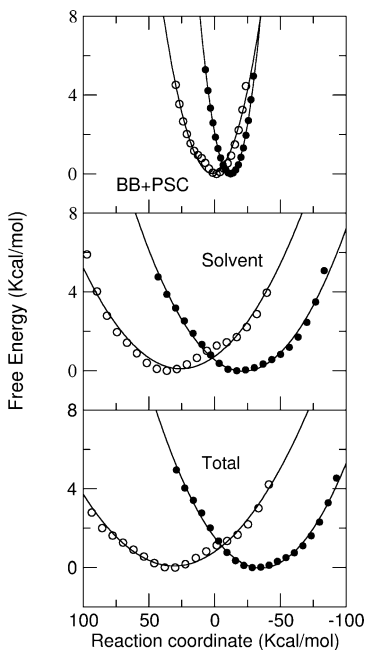


Figure 4. Calculated free energy curves for reactant (○) and product (●) systems assuming zero driving force between the reactant and product. The solid lines are corresponding parabolic fits of the calculated data. The top panel is for the protein backbone and polar side chains (BB+PSC); the middle panel is for the solvent plus counterions and charged side chain (Solvent); and the bottom panel is for the total system (Total).

TABLE 1: Calculated Thermodynamic Parameters (kcal/mol)

	ΔG°	λ_P	λ_R	λ	$\Delta G^\ddagger a$
fit	-0.7 ± 0.5	5.4 ± 5	3.4 ± 3	4.3 ± 3	0.8 ± 0.7 (1.1 ± 0.7)
Gaussian	-0.6 ± 0.4	5.4 ± 3	3.6 ± 2	4.3 ± 3	0.8 ± 0.6 (1.0 ± 0.6)

^a Numbers in parentheses assume $\Delta G^\circ = 0$.

The free energy curves of an intramolecular electron-transfer reaction assuming no driving force for Ca Fd were calculated from the histograms by using eq 6 and the calculated curves were fitted to parabolas (Figure 4, bottom panel). The free energy curves for the backbone and polar side chains of the protein (Figure 4, top panel) and the solvent plus counterions and charged side chains of the protein (Figure 4, middle panel) were also constructed. All the curves were fit well by the parabolas. However, the reactant and product curves for the backbone and polar side chains of the protein have different curvatures (as also reflected in the histograms of Figure 3), despite the quasi-2-fold symmetry of the protein fold with respect to the two iron–sulfur centers. This is discussed more fully in the Discussion section.

The various parameters describing the intramolecular electron transfer of Ca Fd were calculated from the fitted parabola free energy curves. The calculated driving force for the total system is $\Delta G^\circ = -0.7$ kcal/mol (in the Discussion following this section, calculated energies compared with experiment are given in both kcal/mol and meV). The other electron-transfer quantities were calculated both with the calculated driving force and with $\Delta G^\circ = 0$ (Table 1), since the error in the calculated driving force is high. When the driving force was considered to be zero, $\Delta G^\ddagger = 1.1$ kcal/mol, while when the driving force was added, $\Delta G^\ddagger = 0.8$ kcal/mol. From the parabolic shape of the curves, λ is independent of ΔG° so for the total system, $\lambda = 4.3$ kcal/

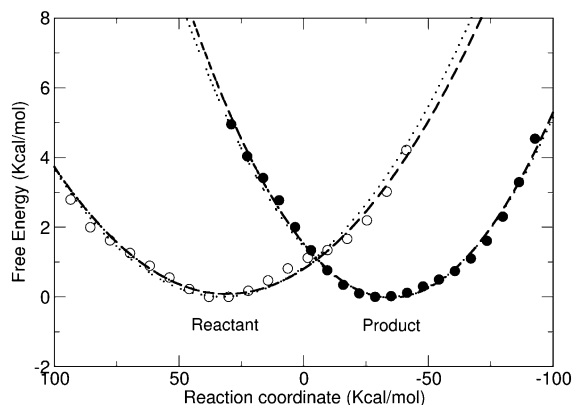


Figure 5. Calculated free energy curves for the total system assuming zero driving force. Dashed lines are the fitted parabolas, obtained from simulated data (○ and ●), and dotted lines are the Gaussian parabolas.

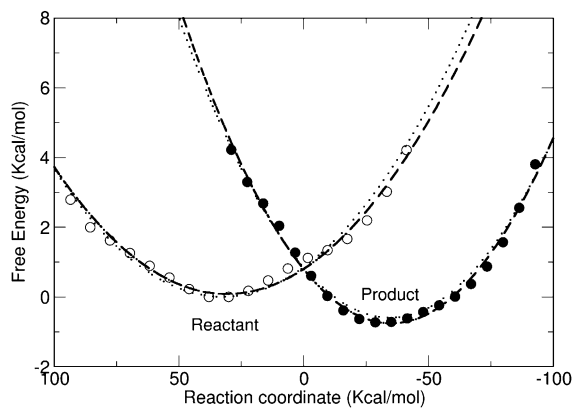


Figure 6. Calculated free energy curves for the total system assuming nonzero driving force (Table 1). Dashed lines are the fitted parabolas, obtained from simulated data (○ and ●), and dotted lines are the Gaussian parabolas.

mol. Approximate values for the activation and reorganization energies due to the backbone and polar side chains ($\Delta G^\ddagger = 0.4 \pm 0.2$ and $\lambda = 1.7 \pm 1$ kcal/mol, respectively) and the solvent plus counterions and charged side chains ($\Delta G^\ddagger = 0.6 \pm 0.4$ and $\lambda = 2.6 \pm 2$ kcal/mol, respectively) were also calculated from the fitted curves for the two components. Since $\lambda_R = 3.4$ kcal/mol and $\lambda_P = 5.4$ kcal/mol, the average $\lambda = 4.4$ kcal/mol is close to the value from the Marcus relationship.

Gaussian Mean Parabolas Overall, the constructed Gaussian parabolas are very similar to the free energy curves obtained by the least-squares fit to the histograms (Figures 5 and 6). The calculated mean values of reaction coordinates for reactant and product are $X_R = 32.5$ kcal/mol and $X_P = -34.6$ kcal/mol, with root-mean-square dynamic fluctuations of $\sigma_R = 19.3$ kcal/mol and $\sigma_P = 15.8$ kcal/mol, respectively, were also used to calculate the electron-transfer parameters (Table 1). The calculated reorganization energies are $\lambda_R = 3.6$ kcal/mol from the force constant $k_R = 1.6 \times 10^{-3}$ mol/kcal, and $\lambda_P = 5.4$ kcal/mol from the force constant $k_P = 2.4 \times 10^{-3}$ mol/kcal. The average of the root-mean-square dynamical fluctuations of the reaction coordinates for reactant and product systems, $\sigma = \sqrt{(\sigma_R^2 + \sigma_P^2)/2} = 17.6$ kcal/mol, gives a calculated average force constant of 1.9×10^{-3} mol/kcal so that the average reorganization energy is 4.3 mol/kcal. The calculated driving force is $\Delta G^\circ = -0.6$ kcal/mol by using eq 16.

Electron-Transfer Rate. According to Marcus theory, the rate constant for a nonadiabatic ET process is given by¹

$$\kappa_{\text{et}} = (2\pi/\hbar T_{\text{DA}})^2 (4\pi\lambda k_{\text{B}}T)^{-1/2} \exp[-(\lambda + \Delta G^\circ)^2/(4\lambda k_{\text{B}}T)] \quad (17)$$

Supposing the intervening protein is a homogeneous medium and $T_{\text{DA}} = T_{\text{DA}}^0 \exp[-\beta(r - r_0)]$, where T_{DA}^0 is the electronic coupling at van der Waals contact (r_0) and $\beta = 1.4 \text{ \AA}^{-1}$ is the distant decay coefficient, the ET rate can be simplified at room temperature to^{3,15,45}

$$\log \kappa_{\text{et}} = 15.2 - 0.6r - 3.1(\lambda + \Delta G^\circ)^2/\lambda \quad (18)$$

where r is the distance in Å between donor and acceptor and λ and ΔG° are in eV. For the Ca Fd, the shortest distance of 10 Å between the Fe atoms and the center-to-center distance of 12 Å between two [4Fe–4S] clusters were used in the calculations.¹⁵ The experimental work by Moulis's group used a distance of 10 Å.¹⁵

The rate of electron transfer, κ_{et} , was calculated with and without the inclusion of the calculated driving force assuming r is 10 Å. Since this calculation only gives the outer sphere reorganization energy, a value of 0.64 eV⁴⁶ was estimated for the inner sphere reorganization energy so that the total reorganization energy, which is approximately the sum of the inner and outer sphere reorganization energies, was about 0.8 eV. For the fit or Gaussian parabolas, κ_{et} is about $8 \times 10^6 \text{ s}^{-1}$ if the calculated driving force was included and about $5 \times 10^6 \text{ s}^{-1}$ if the driving force was set to zero.

Discussion

Overall, the histograms show that the free energy curve is parabolic. The harmonic nature of the free energy curve is consistent with findings in other proteins.¹³ Furthermore, there is an excellent agreement between the values calculated from the least-squares fit to the histograms and the values obtained by the Gaussian parabola method. This indicates that the Gaussian parabola method is an accurate and simple method of extracting the various electron-transfer parameters directly from the simulation.

The parabolas for the reactants and products show different curvatures with a larger k for the products than the reactants. This actually leads to the overall negative reaction free energy. This seems contrary to the pseudosymmetry of ferredoxin. However, the reason may lie in part in the fact that the symmetry is not complete. To have a more completely symmetrical molecule, the N and C termini, which lie near cluster 2, would have to be connected by an additional three residues, or in other words, cluster 2 is more solvent accessible. Presumably, the more polar environment around cluster 2 leads to a greater dielectric behavior for the products where the extra electron is on cluster 2 in which the k is larger and the mean is shifted further away from $\Delta V = 0$. Furthermore, there appears to be a nonlinear response behavior in the reactants as indicated by the tail in the reactant histogram. Since the protein around a cluster expands when the extra electron is on that cluster, this tail may be due to a slightly greater probability of "expansion" around cluster 2 in the reactants (in which the electron is in cluster 1) due to motion of N and C termini. This means a larger population of product-like configuration in the reactant simulations.

The calculated driving force in the electron transfer is relatively small ($-0.7 \pm 0.5 \text{ kcal/mol} = -30 \pm 21 \text{ meV}$, Table 1), which is in reasonable agreement with recent experimental estimates ($-0.14 \text{ kcal/mol} = -6 \text{ meV}$)¹⁵ and is also consistent

with the fact that both [4Fe–4S] redox sites in Ca Fd have similar reduction potentials of $\sim 420 \text{ mV}$.

The calculated reorganization energy for the entire system is relatively low (4.3 kcal/mol = 186 meV), indicating fast intramolecular electron transfer between the two [4Fe–4S] clusters of Ca Fd. This value is lower than the value of 0.5 to 1 eV estimated in other proteins via experiment.¹⁵ The separate calculated contributions of the polar part of the protein and the aqueous solution plus charged side chains are not additive since there is obviously coupling between these contributions, but can be used as an estimate of the relative contributions. The reorganization energy due to the protein backbone and polar side chains alone (1.7 kcal/mol = 74 meV) is relatively low, which is consistent with the fact that the protein backbone is more constrained and less able to reorganize upon transfer of an electron between two [4Fe–4S] redox sites. Likewise, the reorganization energy due to the aqueous solution (2.6 kcal/mol = 113 meV) is relatively higher, which is consistent with the fact that the solvent and counterions can reorganize more easily than the protein upon transfer of the electron from one redox site to the other. These results indicate that protein decreases the overall reorganization energy relative to a pure solvent environment. This is consistent with the findings for cytochrome *c* by Warshel and co-workers, where the reorganization energy was shown to be significantly smaller in proteins than in water.⁴⁷

Finally, the estimated rate here for the intramolecular electron transfer in Ca Fd is on the order of 10^6 s^{-1} , which is comparable to the experimental rate, also on the order of 10^6 s^{-1} .¹⁵ This rate was calculated by using the same distance r and the same electronic coupling decay coefficient, β , in T_{DA} as was used in the experimental work of Moulis,¹⁵ which assumed that it is independent of the structural features of the intervening protein matrix and so the parameters were chosen based on values from other proteins. In Moulis's work, good agreement with the measured rate constants was obtained with these parameters when λ was chosen as 0.5 (giving a rate of 3.5×10^7) to 1.0 eV (giving a rate of 1.0×10^6), which are values based on other proteins.¹⁵ However, values of λ between 0.5 and 1.0 eV imply that the rate should increase 30% to 90%, respectively, in the temperature range of 283 to 308 K used in the experiment whereas the measured rates suggested that the rate was temperature independent. Since the inner sphere reorganization energy has been estimated to be from 0.33⁴⁸ to 0.64⁴⁶ eV and there is uncertainty in the values of r and β as well, the total reorganization energy might actually be smaller. Regardless, our results appear consistent with Moulis's work, which indicates that the outer sphere reorganization is small.

Another important aspect of this work is that it is demonstrated here that the intramolecular electron-transfer properties can be estimated by using molecular dynamics simulations. In particular, the use of the Gaussian parabolas rather than the fit parabolas is an accurate way of calculating the parameters. More fundamentally, this is a demonstration of the linear response of a system with Gaussian fluctuations. Thus, since the histograms show that the fluctuations in the polarization are Gaussian, the polarization energy is linear.

Conclusions

The results presented here show that the electron-transfer properties of Ca Fd can be calculated by using MD simulations. First, the calculated driving force between the two [4Fe–4S] redox sites in Ca Fd is very small, in agreement with the experimental measurement and consistent with the fact that the

reduction potentials of the both redox sites in Ca Fd are highly similar (~ 420 mV). Second, the calculated outer sphere reorganization energies are relatively small, suggesting that the intramolecular electron transfer between the two [4Fe–4S] clusters is fast. Third, our estimated rate is in good agreement with experiment. Finally, the Gaussian parabola method is shown to be a more efficient method for obtaining the electron-transfer properties than fitting parabolas to free energy curves from histograms.

Acknowledgment. This work was supported by grants from the National Institutes of Health (GM45303). Computer time was provided by the National Partnership for Advanced Computational Infrastructure at the Texas Advanced Computing Center under NSF cooperative agreement MCB990010. The views and conclusions contained in this document are those of the authors and should not be interpreted as necessarily representing the official policies or endorsements, either expressed or implied, of the U.S. Government.

References and Notes

- (1) Marcus, R. A.; Sutin, N. *Biochim. Biophys. Acta* **1985**, *811*, 265.
- (2) Levich, V. G. *Adv. Electrochem. Electrochem. Eng.* **1966**, *4*, 349.
- (3) Warshel, A. *J. Phys. Chem.* **1982**, *86*, 2218.
- (4) Churg, A. K.; Weiss, R. M.; Warshel, A.; Takano, T. *J. Phys. Chem.* **1983**, *87*, 1683.
- (5) Hwang, J.-K.; Warshel, A. *J. Am. Chem. Soc.* **1987**, *109*, 715.
- (6) King, G.; Warshel, A. *J. Chem. Phys.* **1990**, *93*, 8682.
- (7) Kuharski, R. A.; Bader, J. S.; Chandler, D.; Sprik, M.; Klein, M. L.; Impey, R. W. *J. Chem. Phys.* **1988**, *89*, 3248.
- (8) Chandler, D.; Kuharski, R. A. *Faraday Discuss. Chem. Soc.* **1988**, *85*, 329.
- (9) Yelle, R. B.; Ichiye, T. *J. Phys. Chem. B* **1997**, *101*, 4127.
- (10) Yelle, R. B. Theoretical Studies of the Electron-Transfer Properties of Rubredoxin. Ph.D. (Biochemistry) Thesis, Washington State University, 1996.
- (11) Creighton, S.; Hwang, J.-K.; Warshel, A.; Parson, W. W.; Norris, J. *Biochemistry* **1988**, *27*, 774.
- (12) Marchi, M.; Gehlen, J. N.; Chandler, D.; Newton, M. *J. Am. Chem. Soc.* **1993**, *115*, 4178.
- (13) Parson, W. W.; Chu, Z. T.; Warshel, A. *Biophys. J.* **1998**, *74*, 182.
- (14) Voet, D.; Voet, J. G. *Biochemistry*, 2nd ed.; John Wiley & Sons: New York, 1995.
- (15) Kyritsis, P.; Huber, J. G.; Quinkal, I.; Gaillard, J.; Moulis, J.-M. *Biochemistry* **1997**, *36*, 7839.
- (16) Bechtold, R. C.; Kuehn, C. L.; Isied, S. S. *Nature* **1986**, *322*, 286.
- (17) Yocom, K. M.; Shelton, J. B.; Shelton, J. R.; Schroeder, W. A.; Worosila, G.; Isied, S. S.; Bordignon, E.; Gray, H. B. *Proc. Natl. Acad. Sci. U.S.A.* **1982**, *79*, 7052.
- (18) Gao-Sheridan, H. S.; Pershad, H. R.; Armstrong, F. A.; Burgess, B. K. *J. Biol. Chem.* **1998**, *273*, 5514.
- (19) Chen, K. S.; Hirst, J.; Camba, R.; Bonagura, C. A.; Stout, C. D.; Burgess, B. K.; Armstrong, F. A. *Nature* **2000**, *405*, 814.
- (20) Moulis, J. M.; Davasse, V. *Biochemistry* **1995**, *34*, 16781.
- (21) Breese, K.; Fuchs, G. *Eur. J. Biochem.* **1998**, *251*, 916.
- (22) Adman, E.; Sieker, L. C.; Jensen, L. H. *J. Biol. Chem.* **1973**, *248*, 3987.
- (23) Matsubara, H.; Saeki, K. Structural and functional diversity of ferredoxins and related proteins. In *Iron–Sulfur Proteins*; Cammack, R., Ed.; Academic Press: San Diego, CA, 1992; Vol. 38, p 223.
- (24) Blanchard, L.; Payan, F.; Qian, M.; Haser, R.; Noailly, M.; Bruschi, M.; Guerlesquin, F. *Biochim. Biophys. Acta* **1993**, *1144*, 124.
- (25) Bertini, I.; Brigandt, F.; Luchinat, C.; Messori, L.; Monnanni, R.; Scozzafava, A.; Vallini, G. *Eur. J. Biochem.* **1992**, *204*, 831.
- (26) Cammack, R. *Adv. Inorg. Chem.* **1992**, *38*, 281.
- (27) Kyritsis, P.; Hatzfeld, O. O.; Link, T. A.; Moulis, J.-M. *J. Biol. Chem.* **1998**, *273*, 15404.
- (28) Bernstein, F. C.; Koetzle, T. F.; Williams, G. J. B.; Meyer, E. F., Jr.; Brice, M. D.; Rodgers, J. R.; Kennard, O.; Shimanouchi, T.; Tasumi, M. *J. Mol. Biol.* **1977**, *112*, 535.
- (29) Cusanovich, M. A. Intracomplex and intramolecular electron transfer in macromolecules. In *Macromolecular Complexes*; Tschida, E., Ed.; John Wiley & Sons: New York, 1991; p 213.
- (30) Mauk, A. G. *Essays Biochem.* **1999**, *34*, 101.
- (31) Dauter, Z.; Wilson, K. S.; Sieker, L. C.; Meyer, J.; Moulis, J. M. *Biochemistry* **1997**, *36*, 16065.
- (32) Beck, B. W.; Koerner, J. B.; Ichiye, T. *J. Phys. Chem. B* **1999**, *103*, 8006.
- (33) Backes, G.; Mino, Y.; Loehr, T. M.; Meyer, T. E.; Cusanovich, M. A.; Sweeny, W. V.; Adman, E. T.; Sanders-Loehr, J. *J. Am. Chem. Soc.* **1991**, *113*, 2055.
- (34) Marcus, R. A. Nobel lecture (www.nobel.se/chemistry/laureates/1992/marcus-lecture.html), 1992.
- (35) Brooks, B. R.; Brucolieri, R. E.; Olafson, B. D.; States, D. J.; Swaminathan, S.; Karplus, M. *J. Comput. Chem.* **1983**, *4*, 187.
- (36) Feller, S. E.; Pastor, R. W.; Rojnuckarin, A.; Bogusz, S.; Brooks, B. R. *J. Phys. Chem.* **1996**, *100*, 17011.
- (37) Ryckaert, J. P.; Ciccotti, G.; Berendsen, H. J. C. *J. Comput. Phys.* **1977**, *23*, 327.
- (38) Yelle, R. B.; Park, N.-S.; Ichiye, T. *Proteins: Struct. Funct. Genet.* **1995**, *22*, 154.
- (39) Jorgensen, W. L. *J. Am. Chem. Soc.* **1981**, *103*, 335.
- (40) Pettitt, B. M.; Rossky, P. J. *J. Chem. Phys.* **1986**, *84*, 5836.
- (41) Hyun, J.-K.; Ichiye, T. *J. Phys. Chem. B* **1997**, *101*, 3596.
- (42) Hyun, J.-K.; Ichiye, T. *J. Chem. Phys.* **1998**, *109*, 1074.
- (43) Ichiye, T. *J. Chem. Phys.* **1996**, *104*, 7561.
- (44) Dolan, E. A.; Yelle, R. B.; Beck, B. W.; Fischer, J. T.; Ichiye, T. *Biophys. J.* **2004**, *86*, 2030.
- (45) Moser, C. C.; Page, C. C.; Farid, R.; Dutton, P. L. *J. Bioenerg. Biomembr.* **1995**, *27*, 263.
- (46) Sigfridsson, E.; Olsson, M. H. M.; Ryde, U. *Inorg. Chem.* **2001**, *40*, 2509.
- (47) Muegge, I.; Qi, P. X.; Wand, A. J.; Chu, Z. T.; Warshel, A. *J. Phys. Chem.* **1997**, *101*, 825.
- (48) Reynolds, J. G.; Coyle, C. L.; Holm, R. H. *J. Am. Chem. Soc.* **1980**, *102*, 4350.